On Robust Capon Beamforming and Diagonal Loading

Jian Li, *Senior Member, IEEE*, Petre Stoica, *Fellow, IEEE*, and Zhisong Wang, *Student Member, IEEE*

Abstract—The Capon beamformer has better resolution and much better interference rejection capability than the standard (data-independent) beamformer, provided that the array steering vector corresponding to the signal of interest (SOI) is accurately known. However, whenever the knowledge of the SOI steering vector is imprecise (as is often the case in practice), the performance of the Capon beamformer may become worse than that of the standard beamformer. Diagonal loading (including its extended versions) has been a popular approach to improve the robustness of the Capon beamformer. In this paper, we show that a natural extension of the Capon beamformer to the case of uncertain steering vectors also belongs to the class of diagonal loading approaches, but the amount of diagonal loading can be precisely calculated based on the uncertainty set of the steering vector. The proposed robust Capon beamformer can be efficiently computed at a comparable cost with that of the standard Capon beamformer. Its excellent performance for SOI power estimation is demonstrated via a number of numerical examples.

Index Terms—Adaptive arrays, array errors, diagonal loading, robust adaptive beamforming, robust Capon beamforming, signal power estimation, steering vector uncertainty.

I. INTRODUCTION

BEAMFORMING is a ubiquitous task in array signal processing with applications, among others, in radar, sonar, acoustics, astronomy, seismology, communications, and medical imaging. Without loss of generality, we consider herein beamforming in array processing applications. The standard data-independent beamformers include the delay-and-sum approach as well as methods based on various data-independent weight vectors for sidelobe control [1], [2]. The data-dependent Capon beamformer adaptively selects the weight vector to minimize the array output power subject to the linear constraint that the signal of interest (SOI) does not suffer from any distortion [3], [4]. The Capon beamformer has a better resolution and much better interference rejection capability than the data-independent beamformer, provided that the array steering vector corresponding to the SOI is accurately known. However, the knowledge of the SOI steering vector

can be imprecise, which is often the case in practice due to the differences between the assumed signal arrival angle and the true arrival angle or between the assumed array response and the true array response (array calibration errors). Whenever this happens, the performance of the Capon beamformer may become worse than that of the standard beamformers [5], [6].

Many approaches have been proposed during the past three decades to improve the robustness of the Capon beamformer. Indeed, the literature on robust adaptive beamforming is quite extensive. We provide a brief review of this literature below. For more detailed recent critical reviews of this literature, see [2] and [7]–[9].

To account for the array steering vector errors, additional linear constraints, including point and derivative constraints, can be imposed to improve the robustness of the Capon beamformer (see, e.g., [10]–[13] and the references therein). However, these constraints are not explicitly related to the uncertainty of the array steering vector. Moreover, for every additional linear constraint imposed, the beamformer loses one degree of freedom (DOF) for interference suppression. It has been shown that these constraints belong to the class of covariance matrix tapering approaches (see [14] and the references therein).

Diagonal loading (including its extended versions) has been a popular approach to improve the robustness of the Capon beamformer (see, e.g., [15]–[23] and the references therein for more early suggested methods). The diagonal loading approaches are derived by imposing an additional quadratic constraint either on the Euclidean norm of the weight vector itself or on its difference from a desired weight vector [15]–[18]. Sometimes, diagonal loading is also proposed to alleviate various problems of using the array sample covariance matrix [19] and to better control the peak sidelobe responses [21]. However, for most of these methods, it is not clear how to choose the diagonal loading based on the uncertainty of the array steering vector.

The subspace-based adaptive beamforming methods (see, e.g., [22], [24], and the references therein) require the knowledge of the noise covariance matrix. Hence, they are sensitive to the imprecise knowledge of the noise covariance matrix in addition to the array steering vector error. Making these methods robust against the array steering vector error will not cure their problem of being sensitive to the imprecise knowledge of the noise covariance matrix.

Even from the above brief review, it is clear that most of the early suggested methods are rather *ad hoc* in that the choice of their parameters is not directly related to the uncertainty of the steering vector. Only recently have some methods with a clear theoretical background been proposed; see, e.g., [8], [9], [25], and [26], which, unlike the early methods, make explicit use of

an uncertainty set of the array steering vector. In [25], a polyhedron is used to describe the uncertainty set, whereas spherical and ellipsoidal (including flat ellipsoidal) uncertainty sets are considered in [8], [9], and [26]. The robust Capon beamforming approaches presented in [8] and [9] couple the formulation of the standard Capon beamformer (SCB) in [3] with a spherical or ellipsoidal uncertainty set of the array steering vector. Interestingly, they turn out to belong to the class of diagonal loading approaches, but the amount of diagonal loading can be calculated precisely based on the ellipsoidal uncertainty set, as explained later in the paper.

Like the approaches in [8] and [9], the robust Capon beamformer (RCB) we proposed in [26] also has a firm theoretical basis and is a natural extension of the Capon beamformer to the case of uncertain steering vectors. However, our RCB approach is different from those in [8] and [9] in that we couple the formulation of SCB in [27] with an ellipsoidal uncertainty set. Our RCB gives a simple way of eliminating the scaling ambiguity when estimating the power of the desired signal, whereas the approaches in [8] and [9] did not consider the scaling ambiguity problem (see below for details on this important aspect).

In this paper, we show how to efficiently compute our robust Capon beamformer by using the Lagrange multiplier methodology. It turns out that our RCB also belongs to the class of diagonal loading approaches and that the amount of diagonal loading can be precisely calculated based on the ellipsoidal uncertainty set of the array steering vector. In fact, we prove that despite the apparent differences between our RCB approach and those in [8] and [9], our RCB gives the same weight vector as the RCBs presented in [8] and [9], yet our RCB is simpler and computationally more efficient. Moreover, we also explain how the RCBs presented in [8] and [9] can be modified to eliminate the scaling ambiguity problem when estimating the power of the desired signal. Numerical examples are presented to demonstrate the effectiveness of our RCB for SOI power estimation: a task that occurs frequently in applications including radar, sonar, and acoustic imaging.

First, we consider the case of nondegenerate ellipsoidal constraints on the steering vector and then the case of flat ellipsoidal constraints. These two cases are treated separately due to the differences in their detailed computational steps as well as in the possible values of the associated Lagrange multipliers. In Section II, we formulate the problem of interest. In Section III, we present the RCB under the nondegenerate and flat ellipsoidal constraints on the steering vector. Numerical examples illustrating the performance of our RCB are given in Section IV. Finally, Section V contains the conclusions.

II. PROBLEM FORMULATION

Consider an array comprising M sensors, and let $\mathbf{R}$ denote the theoretical covariance matrix of the array output vector. We assume that $\mathbf{R} > 0$ (positive definite) has the following form:

$$\mathbf{R} = \sigma_0^2 \mathbf{a}_0 \mathbf{a}_0^* + \sum_{k=1}^{K} \sigma_k^2 \mathbf{a}_k \mathbf{a}_k^* + \mathbf{Q} \tag{1}$$

where $(\sigma_0^2, \{\sigma_k^2\}_{k=1}^K)$ are the powers of the $(K+1)$ uncorrelated signals impinging on the array, $(\mathbf{a}_0, \{\mathbf{a}_k\}_{k=1}^K)$ are the so-called steering vectors that are functions of the location parameters of the sources emitting the signals [e.g., their directions of arrival (DOAs)], $(\cdot)^*$ denotes the conjugate transpose, and $\mathbf{Q}$ is the noise covariance matrix [the "noise" comprises nondirectional signals, and hence, $\mathbf{Q}$ usually has full rank, as opposed to the other terms in (1), whose rank is equal to one]. In what follows, we assume that the first term in (1) corresponds to the SOI and the remaining rank-one terms to K interferences. To avoid ambiguities, we assume that

$$\|\mathbf{a}_0\|^2 = M \tag{2}$$

where $\| \cdot \|$ denotes the Euclidean norm. We note that the above expression for $\mathbf{R}$ holds for both narrowband and wideband signals; in the former case, $\mathbf{R}$ is the covariance matrix at the center frequency, and in the latter, $\mathbf{R}$ is the covariance matrix at the center of a given frequency bin. In practical applications, $\mathbf{R}$ is replaced by the sample covariance matrix $\hat{\mathbf{R}}$, where

$$\hat{\mathbf{R}} = \frac{1}{N} \sum_{n=1}^{N} \mathbf{x}_n \mathbf{x}_n^* \tag{3}$$

with N denoting the number of snapshots and $\mathbf{x}_n$ representing the nth snapshot.

The *robust beamforming problem* with which we will deal in this paper can now be briefly stated as follows: Extend the Capon beamformer to be able to accurately determine the power of SOI even when only an imprecise knowledge of its steering vector $\mathbf{a}_0$ is available. More specifically, we assume that the only knowledge we have about $\mathbf{a}_0$ is that it belongs to the following uncertainty ellipsoid:

$$[\mathbf{a}_0 - \bar{\mathbf{a}}]^* \mathbf{C}^{-1} [\mathbf{a}_0 - \bar{\mathbf{a}}] \leq 1 \tag{4}$$

where $\bar{\mathbf{a}}$ and $\mathbf{C}$ (a positive definite matrix) are given. The case of a flat ellipsoidal uncertainty set is considered in Section III-B. In this paper, we focus on SOI power estimation problem, but the robust beamforming approach we present herein can also be used for other applications including signal waveform estimation [8], [9], [28].

III. ROBUST CAPON BEAMFORMING

The common formulation of the beamforming problem that leads to the SCB is as follows (see, e.g., [1], [3], [4]).

a) Determine the $M \times 1$ vector $\mathbf{w}_0$ that is the solution to the following linearly constrained quadratic problem:

$$\min_{\mathbf{w}} \mathbf{w}^* \mathbf{R} \mathbf{w} \qquad \text{subject to } \mathbf{w}^* \mathbf{a}_0 = 1. \tag{5}$$

b) Use $\mathbf{w}_0^* \mathbf{R} \mathbf{w}_0$ as an estimate of σ_0^2.

The solution to (5) is easily derived:

$$\mathbf{w}_0 = \frac{\mathbf{R}^{-1} \mathbf{a}_0}{\mathbf{a}_0^* \mathbf{R}^{-1} \mathbf{a}_0}. \tag{6}$$

Using (6) in Step b) above yields the following estimate of σ_0^2:

$$\tilde{\sigma}_0^2 = \frac{1}{\mathbf{a}_0^* \mathbf{R}^{-1} \mathbf{a}_0}. \tag{7}$$

A. Nondegenerate Ellipsoidal Uncertainty Set

To derive our robust Capon beamforming approach, we use the reformulation of the Capon beamforming problem in [27] to which we append the uncertainty set in (4) (see [26]). Proceeding in this way, we *directly* obtain a robust estimate of σ_0^2, without any intermediate calculation of a vector $\mathbf{w}$ [26]:

$$\max_{\sigma^2, \mathbf{a}} \sigma^2 \qquad \text{subject to } \mathbf{R} - \sigma^2 \mathbf{a}\mathbf{a}^* \geq 0$$

$$\text{for any } \mathbf{a} \text{ satisfying } (\mathbf{a} - \bar{\mathbf{a}})^* \mathbf{C}^{-1} (\mathbf{a} - \bar{\mathbf{a}}) \leq 1 \tag{8}$$

(where $\bar{\mathbf{a}}$ and $\mathbf{C}$ are given). Note that the first line above can be interpreted as a *covariance fitting problem*: Given $\mathbf{R}$ and $\mathbf{a}$, we wish to determine the largest possible SOI term $\sigma^2 \mathbf{a}\mathbf{a}^*$ that can be a part of $\mathbf{R}$ under the natural constraint that the residual covariance matrix be positive semidefinite. The RCB problem in (8) can be readily reformulated as a semi-definite program [26], which requires $O(\rho M^6)$ flops if SeDuMi type of software [29] is used to solve it, where ρ is the number of iterations. However, the approach we present below only requires $O(M^3)$ flops.

For any given $\mathbf{a}$, the solution $\hat{\sigma}_0^2$ to (8) is indeed given by the counterpart of (7) with $\mathbf{a}_0$ replaced by $\mathbf{a}$, as shown in [26]. Hence, (8) can be reduced to the following problem:

$$\min_{\mathbf{a}} \mathbf{a}^* \mathbf{R}^{-1} \mathbf{a} \qquad \text{subject to } (\mathbf{a} - \bar{\mathbf{a}})^* \mathbf{C}^{-1} (\mathbf{a} - \bar{\mathbf{a}}) \leq 1. \tag{9}$$

Note that we can decompose any matrix $\mathbf{C} > 0$ in the form

$$\mathbf{C}^{-1} = \frac{1}{\epsilon} \mathbf{D}^* \mathbf{D} \tag{10}$$

where for some $\epsilon > 0$

$$\mathbf{D} = \sqrt{\epsilon} \mathbf{C}^{-1/2}. \tag{11}$$

Let

$$\breve{\mathbf{a}} = \mathbf{D}\mathbf{a}, \quad \bar{\breve{\mathbf{a}}} = \mathbf{D}\bar{\mathbf{a}}, \quad \breve{\mathbf{R}} = \mathbf{D}\mathbf{R}\mathbf{D}^*. \tag{12}$$

Then, (9) becomes

$$\min_{\breve{\mathbf{a}}} \breve{\mathbf{a}}^* \breve{\mathbf{R}}^{-1} \breve{\mathbf{a}} \qquad \text{subject to } \left\| \breve{\mathbf{a}} - \bar{\breve{\mathbf{a}}} \right\|^2 \leq \epsilon. \tag{13}$$

Hence, without loss of generality, we will consider solving (9) for $\mathbf{C} = \epsilon \mathbf{I}$, i.e., solving the following quadratic optimization problem under a spherical constraint:

$$\min_{\mathbf{a}} \mathbf{a}^* \mathbf{R}^{-1} \mathbf{a} \qquad \text{subject to } \|\mathbf{a} - \bar{\mathbf{a}}\|^2 \leq \epsilon. \tag{14}$$

To exclude the trivial solution $\mathbf{a} = \mathbf{0}$ to (14), we assume that

$$\|\bar{\mathbf{a}}\|^2 > \epsilon. \tag{15}$$

Because the solution to (14) [under (15)] will evidently occur on the boundary of the constraint set, we can reformulate (14)

as the following quadratic problem with a quadratic equality constraint:

$$\min_{\mathbf{a}} \mathbf{a}^* \mathbf{R}^{-1} \mathbf{a} \qquad \text{subject to } \|\mathbf{a} - \bar{\mathbf{a}}\|^2 = \epsilon. \tag{16}$$

This problem can be solved by using the *Lagrange multiplier methodology*, which is based on the function

$$f = \mathbf{a}^* \mathbf{R}^{-1} \mathbf{a} + \lambda \left(\|\mathbf{a} - \bar{\mathbf{a}}\|^2 - \epsilon \right) \tag{17}$$

where $\lambda \geq 0$ is the Lagrange multiplier [30]. Differentiation of (17) with respect to $\mathbf{a}$ gives the optimal solution $\hat{\mathbf{a}}_0$:

$$\mathbf{R}^{-1} \hat{\mathbf{a}}_0 + \lambda(\hat{\mathbf{a}}_0 - \bar{\mathbf{a}}) = 0. \tag{18}$$

The above equation yields

$$\hat{\mathbf{a}}_0 = \left(\frac{\mathbf{R}^{-1}}{\lambda} + \mathbf{I} \right)^{-1} \bar{\mathbf{a}} \tag{19}$$

$$= \bar{\mathbf{a}} - (\mathbf{I} + \lambda\mathbf{R})^{-1}\bar{\mathbf{a}} \tag{20}$$

where we have used the matrix inversion lemma [1] to obtain the second equality. The Lagrange multiplier $\lambda \geq 0$ is obtained as the solution to the constraint equation

$$g(\lambda) \triangleq \left\| (\mathbf{I} + \lambda\mathbf{R})^{-1}\bar{\mathbf{a}} \right\|^2 = \epsilon. \tag{21}$$

Let

$$\mathbf{R} = \mathbf{U}\mathbf{\Gamma}\mathbf{U}^* \tag{22}$$

where the columns of $\mathbf{U}$ contain the eigenvectors of $\mathbf{R}$, and the diagonal elements of the diagonal matrix $\mathbf{\Gamma}$, $\gamma_1 \geq \gamma_2 \geq \cdots \geq \gamma_M$ are the corresponding eigenvalues. Let

$$\mathbf{z} = \mathbf{U}^* \bar{\mathbf{a}} \tag{23}$$

and let z_m denote the mth element of $\mathbf{z}$. Then, (21) can be written as

$$g(\lambda) = \sum_{m=1}^{M} \frac{|z_m|^2}{(1 + \lambda\gamma_m)^2} = \epsilon. \tag{24}$$

Note that $g(\lambda)$ is a monotonically decreasing function of $\lambda \geq 0$. According to (15) and (21), $g(0) > \epsilon$, and hence, $\lambda \neq 0$. From (24), it is clear that $\lim_{\lambda \to \infty} g(\lambda) = 0 < \epsilon$. Hence, there is a unique solution $\lambda > 0$ to (24). By replacing the γ_m in (24) with γ_M and γ_1, respectively, we can obtain the following tighter upper and lower bounds on the solution $\lambda > 0$ to (24):

$$\frac{\|\bar{\mathbf{a}}\| - \sqrt{\epsilon}}{\gamma_1 \sqrt{\epsilon}} \leq \lambda \leq \frac{\|\bar{\mathbf{a}}\| - \sqrt{\epsilon}}{\gamma_M \sqrt{\epsilon}}. \tag{25}$$

By dropping the 1 in the denominator of (24), we can obtain another upper bound on the solution λ to (24):

$$\lambda < \left(\frac{1}{\epsilon} \sum_{m=1}^{M} \frac{|z_m|^2}{\gamma_m^2} \right)^{1/2}. \tag{26}$$

The upper bound in (26) is usually tighter than the upper bound in (25) but not always. Summing up all these facts shows that

the solution $\lambda > 0$ to (24) is unique and that it belongs to the following interval:

$$\frac{\|\bar{\mathbf{a}}\| - \sqrt{\epsilon}}{\gamma_1 \sqrt{\epsilon}} \leq \lambda \leq \min\left\{ \left(\frac{1}{\epsilon} \sum_{m=1}^{M} \frac{|z_m|^2}{\gamma_m^2} \right)^{1/2}, \frac{\|\bar{\mathbf{a}}\| - \sqrt{\epsilon}}{\gamma_M \sqrt{\epsilon}} \right\}. \tag{27}$$

Once the Lagrange multiplier λ is determined, $\hat{\mathbf{a}}_0$ is determined by using (20), and $\hat{\sigma}_0^2$ is computed by using (7) with $\mathbf{a}_0$ replaced by $\hat{\mathbf{a}}_0$. Hence, the major computational demand of our RCB comes from the eigendecomposition of the Hermitian matrix $\mathbf{R}$, which requires $O(M^3)$ flops. Therefore, the computational complexity of our RCB is comparable with that of the SCB.

Next, observe that both the power and the steering vector of the SOI are treated as unknowns in our robust Capon beamforming formulation [see (8)] and, hence, that there is a "scaling ambiguity" in the SOI covariance term in the sense that $(\sigma^2, \mathbf{a})$ and $(\sigma^2/\alpha, \alpha^{1/2}\mathbf{a})$ (for any $\alpha > 0$) give the same term $\sigma^2 \mathbf{a}\mathbf{a}^*$. To eliminate this ambiguity, we use the knowledge that $\|\mathbf{a}_0\|^2 = M$ [see (2)] and, hence, estimate σ_0^2 as [26]

$$\hat{\hat{\sigma}}_0^2 = \hat{\sigma}_0^2 \|\hat{\mathbf{a}}_0\|^2 / M. \tag{28}$$

The numerical examples in [26] confirm that $\hat{\hat{\sigma}}_0^2$ is a (much) more accurate estimate of σ_0^2 than $\hat{\sigma}_0^2$. To summarize, our proposed RCB approach consists of the following steps.

Proposed RCB (Spherical Constraint):

Step 1) Compute the eigendecomposition of $\mathbf{R}$ (or more practically of $\hat{\mathbf{R}}$).

Step 2) Solve (24) for λ, e.g., by a Newton's method, using the knowledge that the solution is unique and it belongs to the interval in (27).

Step 3) Use the λ obtained in Step 2 to get

$$\hat{\mathbf{a}}_0 = \bar{\mathbf{a}} - \mathbf{U}(\mathbf{I} + \lambda\mathbf{\Gamma})^{-1}\mathbf{U}^*\bar{\mathbf{a}} \tag{29}$$

where the inverse of the diagonal matrix $\mathbf{I} + \lambda\mathbf{\Gamma}$ is easily computed. [Note that (29) is obtained from (20).]

Step 4) Compute $\hat{\sigma}_0^2$ by using

$$\hat{\sigma}_0^2 = \frac{1}{\bar{\mathbf{a}}^* \mathbf{U}\mathbf{\Gamma}(\lambda^{-2}\mathbf{I} + 2\lambda^{-1}\mathbf{\Gamma} + \mathbf{\Gamma}^2)^{-1}\mathbf{U}^*\bar{\mathbf{a}}} \tag{30}$$

where the inverse of $\lambda^{-2}\mathbf{I} + 2\lambda^{-1}\mathbf{\Gamma} + \mathbf{\Gamma}^2$ is also easily computed. Note that $\mathbf{a}_0$ in (7) is replaced by $\hat{\mathbf{a}}_0$ in (19) to obtain (30). Then, use the $\hat{\sigma}_0^2$ in (28) to obtain the estimate of σ_0^2.

We remark that in all of the steps above, we do not need to have $\gamma_m > 0$ for all $m = 1, 2, \ldots, M$. Hence, $\mathbf{R}$ or $\hat{\mathbf{R}}$ can be singular, which means that we can allow $N < M$ to compute $\hat{\mathbf{R}}$.

Unlike our approach, the approaches of [8] and [9] do not provide any *direct* estimate $\hat{\mathbf{a}}_0$. Hence, they do not dispose of a simple way [such as (28)] to eliminate the scaling ambiguity of the SOI power estimation that is likely a problem for all robust beamforming approaches (this problem was in fact ignored in

both [8] and [9]). Note that SOI power estimation is the main goal in many applications including radar, sonar, and acoustic imaging.

In other applications, such as communications, the focus is on SOI waveform estimation. Let $s_0(n)$ denote the waveform of the SOI. Then, once we have estimated the SOI steering vector with our RCB, $s_0(n)$ can be estimated like in the SCB as follows:

$$\hat{s}_0(n) = \hat{\mathbf{w}}_0^* \mathbf{x}_n \tag{31}$$

where $\hat{\mathbf{a}}_0$ in (19) is used to replace $\mathbf{a}_0$ in (6) to obtain $\hat{\mathbf{w}}_0$:

$$\hat{\mathbf{w}}_0 = \frac{\mathbf{R}^{-1}\hat{\mathbf{a}}_0}{\hat{\mathbf{a}}_0^* \mathbf{R}^{-1}\hat{\mathbf{a}}_0} \tag{32}$$

$$= \frac{\left(\mathbf{R} + \frac{1}{\lambda}\mathbf{I}\right)^{-1}\bar{\mathbf{a}}}{\bar{\mathbf{a}}^* \left(\mathbf{R} + \frac{1}{\lambda}\mathbf{I}\right)^{-1} \mathbf{R} \left(\mathbf{R} + \frac{1}{\lambda}\mathbf{I}\right)^{-1}\bar{\mathbf{a}}}. \tag{33}$$

Note that our robust Capon weight vector has the form of diagonal loading except for the real-valued scaling factor in the denominator of (33). However, the scaling factor is not really important since the quality of the SOI waveform estimate is typically expressed by the signal-to-interference-plus-noise ratio (SINR)

$$\text{SINR} = \frac{\sigma_0^2 |\hat{\mathbf{w}}_0^* \mathbf{a}_0|^2}{\hat{\mathbf{w}}_0^* \left(\sum_{k=1}^{K} \sigma_k^2 \mathbf{a}_k \mathbf{a}_k^* + \mathbf{Q} \right) \hat{\mathbf{w}}_0} \tag{34}$$

which is independent of the scaling of the weight vector.

When $\mathbf{C}$ is not a scaled identity matrix, the diagonal loading is added to the weighted matrix $\check{\mathbf{R}}$ defined in (12), and we refer to this case as extended diagonal loading. To exclude the trivial solution $\mathbf{a} = \mathbf{0}$ to (8), we now need to assume, like in (15), that

$$\left\| \bar{\bar{\mathbf{a}}} \right\|^2 > \epsilon \tag{35}$$

which is equivalent to

$$\bar{\mathbf{a}}^* \mathbf{C}^{-1} \bar{\mathbf{a}} > 1. \tag{36}$$

We remark that the discussions above indicate that our robust Capon beamforming approach belongs to the class of (extended) diagonally loaded Capon beamforming approaches. However, unlike earlier approaches, our approach can be used to determine exactly the optimal amount of diagonal loading needed for a given ellipsoidal uncertainty set of the steering vector at a very modest computational cost.

Our approach is different from the recent RCB approaches in [8] and [9]. The latter approaches extended Step a) of the SCB to take into account the fact that when there is uncertainty in $\mathbf{a}_0$, the constraint on $\mathbf{w}^* \mathbf{a}_0$ in (6) should be replaced with a constraint on $\mathbf{w}^* \mathbf{a}$ for any vector $\mathbf{a}$ in the uncertainty set (the constraints on $\mathbf{w}^* \mathbf{a}$ used in [8] and [9] are different from one another); then, the so-obtained $\mathbf{w}$ is used in $\mathbf{w}^* \mathbf{R}\mathbf{w}$ to derive an estimate of σ_0^2, as in Step b) of the SCB. Despite the apparent differences in formulation, we prove in Appendixes A and C that our RCB gives the same weight vector as the RCBs presented in [8] and [9], yet our RCB is computationally more efficient. The approach in [8] requires $O(\rho M^3)$ flops [31], where ρ is the number of iterations, whereas our RCB approach requires $O(M^3)$ flops.

Moreover, our RCB can be readily modified for recursive implementation by adding a new snapshot to $\hat{\mathbf{R}}$ and possibly deleting an old one. By using a recursive eigendecomposition updating method (see, for example, [32], [33], and the references therein) with our RCB, we can update the power and waveform estimates in $O(M^2)$ flops. No results are available so far for efficiently updating the second-order cone program (SOCP) approach in [8]. The approach in [9] can be implemented recursively by updating the eigendecomposition similarly to our RCB. However, the total computational burden is higher than for our RCB, as explained in the next subsection.

We also show in Appendix B that although this aspect was ignored in [8] and [9], the RCBs presented in [8] and [9] can also be modified to eliminate the scaling ambiguity problem that occurs when estimating the SOI power σ_0^2.

B. Flat Ellipsoidal Uncertainty Set

When the uncertainty set for $\mathbf{a}$ is a flat ellipsoid, as is considered in [9] and [28] to make the uncertainty set as tight as possible (assuming that the available *a priori* information allows that), (8) becomes

$$\max_{\sigma^2, \mathbf{a}} \sigma^2 \qquad \text{subject to } \mathbf{R} - \sigma^2 \mathbf{a}\mathbf{a}^* \geq 0$$
$$\mathbf{a} = \mathbf{B}\mathbf{u} + \bar{\mathbf{a}}, \qquad \|\mathbf{u}\| \leq 1 \qquad (37)$$

where $\mathbf{B}$ is an $M \times L$ matrix $(L < M)$ with full column rank, and $\mathbf{u}$ is an $L \times 1$ vector. [When $L = M$, (37) becomes (4) with $\mathbf{C} = \mathbf{B}\mathbf{B}^*$.] Below, we provide a separate treatment of the case of $L < M$ due to the differences from the case of $L = M$ in the possible values of the Lagrange multipliers and the detailed computational steps. The RCB optimization problem in (37) can be reduced to [see (9)]

$$\min_{\mathbf{u}} (\mathbf{B}\mathbf{u} + \bar{\mathbf{a}})^* \mathbf{R}^{-1} (\mathbf{B}\mathbf{u} + \bar{\mathbf{a}}) \qquad \text{subject to } \|\mathbf{u}\| \leq 1. \quad (38)$$

Note that

$$(\mathbf{B}\mathbf{u} + \bar{\mathbf{a}})^* \mathbf{R}^{-1} (\mathbf{B}\mathbf{u} + \bar{\mathbf{a}}) = \mathbf{u}^* \mathbf{B}^* \mathbf{R}^{-1} \mathbf{B}\mathbf{u}$$
$$+ \bar{\mathbf{a}}^* \mathbf{R}^{-1} \mathbf{B}\mathbf{u} + \mathbf{u}^* \mathbf{B}^* \mathbf{R}^{-1} \bar{\mathbf{a}} + \bar{\mathbf{a}}^* \mathbf{R}^{-1} \bar{\mathbf{a}}. \quad (39)$$

Let

$$\check{\mathbf{R}} = \mathbf{B}^* \mathbf{R}^{-1} \mathbf{B} > 0 \qquad (40)$$

and

$$\bar{\bar{\mathbf{a}}} = \mathbf{B}^* \mathbf{R}^{-1} \bar{\mathbf{a}}. \qquad (41)$$

Using (39)–(41) in (38) gives

$$\min_{\mathbf{u}} \mathbf{u}^* \check{\mathbf{R}} \mathbf{u} + \bar{\bar{\mathbf{a}}}^* \mathbf{u} + \mathbf{u}^* \bar{\bar{\mathbf{a}}} \qquad \text{subject to } \|\mathbf{u}\| \leq 1. \quad (42)$$

To avoid the trivial solution $\mathbf{a} = \mathbf{0}$ to the RCB problem in (37), we impose the following condition (assuming $\tilde{\mathbf{u}}$ below exists; otherwise, there is no trivial solution). Let $\tilde{\mathbf{u}}$ be the solution to the equation

$$\mathbf{B}\tilde{\mathbf{u}} + \bar{\mathbf{a}} = \mathbf{0}. \qquad (43)$$

Hence

$$\tilde{\mathbf{u}} = -\mathbf{B}^{\dagger} \bar{\mathbf{a}}. \qquad (44)$$

Then, we require that

$$\bar{\mathbf{a}}^* \mathbf{B}^{\dagger^*} \mathbf{B}^{\dagger} \bar{\mathbf{a}} > 1 \qquad (45)$$

where $\mathbf{B}^{\dagger}$ denotes the Moore–Penrose pseudo-inverse of $\mathbf{B}$.

The *Lagrange multiplier methodology* is based on the function [34]

$$\check{f} = \mathbf{u}^* \check{\mathbf{R}} \mathbf{u} + \bar{\bar{\mathbf{a}}}^* \mathbf{u} + \mathbf{u}^* \bar{\bar{\mathbf{a}}} + \check{\lambda}(\mathbf{u}^* \mathbf{u} - 1) \qquad (46)$$

where $\check{\lambda} \geq 0$ is the Lagrange multiplier [30]. Differentiation of (46) with respect to $\mathbf{u}$ gives

$$\check{\mathbf{R}} \hat{\mathbf{u}} + \bar{\bar{\mathbf{a}}} + \check{\lambda} \hat{\mathbf{u}} = 0 \qquad (47)$$

which yields

$$\hat{\mathbf{u}} = -\left(\check{\mathbf{R}} + \check{\lambda}\mathbf{I}\right)^{-1} \bar{\bar{\mathbf{a}}}. \qquad (48)$$

If $\|\check{\mathbf{R}}^{-1}\bar{\bar{\mathbf{a}}}\| \leq 1$, then the unique solution in (48) with $\check{\lambda} = 0$, which is $\hat{\mathbf{u}} = -\check{\mathbf{R}}^{-1}\bar{\bar{\mathbf{a}}}$, solves (42). If $\|\check{\mathbf{R}}^{-1}\bar{\bar{\mathbf{a}}}\| > 1$, then $\check{\lambda} > 0$ is determined by solving

$$\check{g}\left(\check{\lambda}\right) \triangleq \left\|\left(\check{\mathbf{R}} + \check{\lambda}\mathbf{I}\right)^{-1} \bar{\bar{\mathbf{a}}}\right\|^2 = 1. \qquad (49)$$

Note that $\check{g}(\check{\lambda})$ is a monotonically decreasing function of $\check{\lambda} > 0$. Let

$$\check{\mathbf{R}} = \check{\mathbf{U}} \check{\mathbf{\Gamma}} \check{\mathbf{U}}^* \qquad (50)$$

where the columns of $\check{\mathbf{U}}$ contain the eigenvectors of $\check{\mathbf{R}}$ and the diagonal elements of the diagonal matrix $\check{\mathbf{\Gamma}}$, $\check{\gamma}_1 \geq \check{\gamma}_2 \geq \cdots \geq \check{\gamma}_L$ are the corresponding eigenvalues. Let

$$\check{\mathbf{z}} = \check{\mathbf{U}}^* \bar{\bar{\mathbf{a}}} \qquad (51)$$

and let $\check{z}_l$ denote the lth element of $\check{\mathbf{z}}$. Then

$$\check{g}\left(\check{\lambda}\right) = \sum_{l=1}^{L} \frac{|\check{z}_l|^2}{\left(\check{\gamma}_l + \check{\lambda}\right)^2} = 1. \qquad (52)$$

Note that $\lim_{\check{\lambda} \to \infty} \check{g}(\check{\lambda}) = 0$ and $\check{g}(0) = \|\check{\mathbf{R}}^{-1}\bar{\bar{\mathbf{a}}}\| > 1$. Hence, there is a unique solution to (25) between 0 and ∞. By replacing the $\check{\gamma}_l$ in (52) with $\check{\gamma}_L$ and $\check{\gamma}_1$, respectively, we obtain tighter upper and lower bounds on the solution to (52):

$$\left\|\bar{\bar{\mathbf{a}}}\right\| - \check{\gamma}_1 \leq \check{\lambda} \leq \left\|\bar{\bar{\mathbf{a}}}\right\| - \check{\gamma}_L. \qquad (53)$$

Hence, the solution to (52) can be efficiently determined, e.g., by using the Newton's method, in the above interval. Then, the solution $\check{\lambda}$ to (52) is used in (48) to obtain the $\hat{\mathbf{u}}$ that solves (42).

To summarize, our proposed RCB approach consists of the following steps.

Proposed RCB (Flat Ellipsoidal Constraint):

Step 1) Compute the inverse of $\mathbf{R}$ (or more practically of $\hat{\mathbf{R}}$), and calculate $\check{\mathbf{R}}$ and $\bar{\bar{\mathbf{a}}}$ using (40) and (41), respectively.

Step 2) Compute the eigendecomposition of $\check{\mathbf{R}}$ [see (50)].

Step 3) If $\|\check{\mathbf{R}}^{-1}\bar{\bar{\mathbf{a}}}\| \leq 1$, then set $\check{\lambda} = 0$. If $\|\check{\mathbf{R}}^{-1}\bar{\bar{\mathbf{a}}}\| > 1$, then solve (52) for $\check{\lambda}$, e.g., by a Newton's method, using the knowledge that the solution is unique and it belongs to the interval in (53).
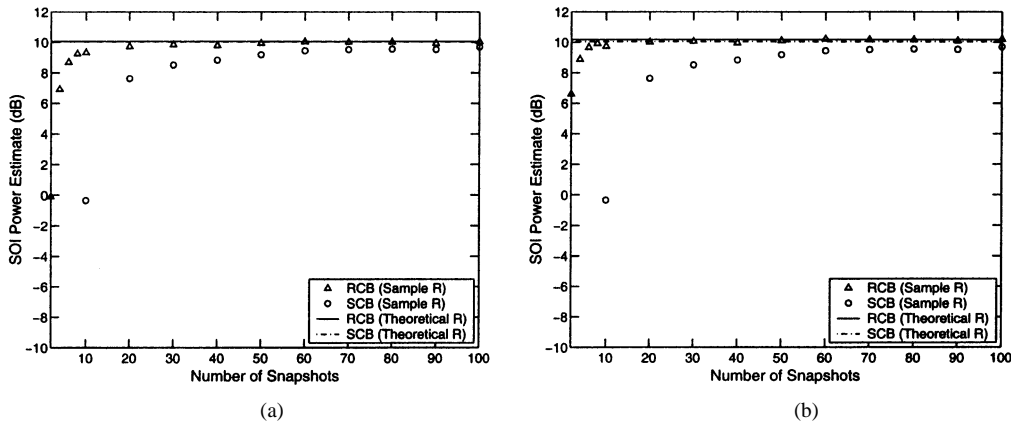
Fig. 1. $\bar{\sigma}_0^2$ (SCB using $\hat{\mathbf{R}}$ and $\mathbf{R}$) and $\hat{\sigma}_0^2$ (RCB using $\hat{\mathbf{R}}$ and $\mathbf{R}$) versus N for (a) $\epsilon = 0.5$ and (b) $\epsilon = 3.5$. The true SOI power is 10 dB, and $\epsilon_0 = 0$ (i.e., no mismatch).

Step 4) Use the $\check{\lambda}$ obtained in Step 3) to get

$$\hat{\mathbf{u}} = -\check{\mathbf{U}} \left(\check{\boldsymbol{\Gamma}} + \check{\lambda} \mathbf{I} \right)^{-1} \check{\mathbf{U}}^* \bar{\mathbf{a}} \qquad (54)$$

[which is obtained from (48)]. Then, use the $\hat{\mathbf{u}}$ to obtain the optimal solution to (37) as

$$\hat{\mathbf{a}}_0 = \mathbf{B}\hat{\mathbf{u}} + \bar{\mathbf{a}}. \qquad (55)$$

Step 5) Compute $\hat{\sigma}_0^2$ by using (7) with $\mathbf{a}_0$ replaced by $\hat{\mathbf{a}}_0$, and then, use the $\hat{\sigma}_0^2$ in (28) to obtain the estimate of σ_0^2.

Hence, under the flat ellipsoidal constraint, the complexity of our RCB is also $O(M^3)$ flops, which is on the same order as for SCB and is mainly due to computing $\mathbf{R}^{-1}$ and the eigendecomposition of $\check{\mathbf{R}}$. If $L \ll M$, then the complexity is mainly due to computing $\mathbf{R}^{-1}$.

For applications such as SOI waveform estimation, we can calculate $\hat{\mathbf{w}}_0$ (assuming $\check{\lambda} \neq 0$) as

$$
\begin{aligned}
\hat{\mathbf{w}}_0 &= \frac{\mathbf{R}^{-1}\hat{\mathbf{a}}_0}{\hat{\mathbf{a}}_0^* \mathbf{R}^{-1}\hat{\mathbf{a}}_0} \\
&= \frac{\left(\mathbf{R} + \frac{1}{\check{\lambda}}\mathbf{B}\mathbf{B}^* \right)^{-1} \bar{\mathbf{a}}}{\bar{\mathbf{a}}^* \left(\mathbf{R} + \frac{1}{\check{\lambda}}\mathbf{B}\mathbf{B}^* \right)^{-1} \mathbf{R} \left(\mathbf{R} + \frac{1}{\check{\lambda}}\mathbf{B}\mathbf{B}^* \right)^{-1} \bar{\mathbf{a}}}.
\end{aligned} \qquad (56)
$$

To obtain (56), we have used the fact [also using (48) in (55)] that

$$
\begin{aligned}
\mathbf{R}^{-1}\hat{\mathbf{a}}_0 &= -\mathbf{R}^{-1}\mathbf{B} \left(\check{\mathbf{R}} + \check{\lambda}\mathbf{I} \right)^{-1} \bar{\mathbf{a}} + \mathbf{R}^{-1}\bar{\mathbf{a}} \\
&= -\mathbf{R}^{-1}\mathbf{B} \left(\mathbf{B}^* \mathbf{R}^{-1}\mathbf{B} + \check{\lambda}\mathbf{I} \right)^{-1} \mathbf{B}^* \mathbf{R}^{-1}\bar{\mathbf{a}} + \mathbf{R}^{-1}\bar{\mathbf{a}} \\
&= \left(\mathbf{R} + \frac{1}{\check{\lambda}}\mathbf{B}\mathbf{B}^* \right)^{-1} \bar{\mathbf{a}}
\end{aligned} \qquad (57)
$$

where the last equality follows from the matrix inversion lemma. Despite the differences in the formulation of our RCB problem and that in [9], we prove in Appendix C that our $\hat{\mathbf{w}}_0$ in (56) and the optimal weight in [9] are identical. Note, however, that to compute $\check{\lambda}$, we need $O(L^3)$ flops, whereas the approach in [9] requires $O(M^3)$ flops (and $L \leq M$).

IV. NUMERICAL EXAMPLES

Our main motivation for studying the RCB problem was an acoustic imaging application in which the goal was to estimate the SOI power in the presence of strong interferences as well as some uncertainty in the SOI steering vector. In all of the examples considered below, we assume a uniform linear array with $M = 10$ sensors and half-wavelength sensor spacing.

First, we consider the effect of the number of snapshots N on the SOI power estimate when the sample covariance matrix $\hat{\mathbf{R}}$ in (3) is used in lieu of the theoretical array covariance matrix $\mathbf{R}$ in both the SCB and RCB. (Whenever $\hat{\mathbf{R}}$ is used instead of $\mathbf{R}$, the average power estimates from 100 Monte Carlo simulations are given. However, the beampatterns shown are obtained using $\hat{\mathbf{R}}$ from one Monte-Carlo realization only.) We assume a spatially white Gaussian noise whose covariance matrix is given by $\mathbf{Q} = \mathbf{I}$. The power of SOI is $\sigma_0^2 = 10$ dB, and the powers of the two ($K = 2$) interferences assumed to be present are $\sigma_1^2 = \sigma_2^2 = 20$ dB. We assume that the steering vector uncertainty is due to the uncertainty in the SOIs direction of arrival θ_0, which we assume to be $\theta_0 + \Delta$. We assume that $\mathbf{a}(\theta_0)$ belongs to the uncertainty set

$$\|\mathbf{a}(\theta_0) - \bar{\mathbf{a}}\|^2 \leq \epsilon; \qquad \bar{\mathbf{a}} = \mathbf{a}(\theta_0 + \Delta) \qquad (58)$$

where ϵ is a user parameter. Let $\epsilon_0 = \|\mathbf{a}(\theta_0) - \bar{\mathbf{a}}\|^2$. Then, choosing $\epsilon = \epsilon_0$ gives the smallest set that includes $\mathbf{a}(\theta_0)$. However, since Δ is unknown in practice, the ϵ we choose may be greater or less than ϵ_0. To show that the choice of ϵ is not a critical issue for our RCB approach, we will present numerical results for several values of ϵ. We assume that the SOIs direction of arrival is $\theta_0 = 0°$ and that the directions of arrival of the interferences are $\theta_1 = 60°$ and $\theta_2 = 80°$.

In Fig. 1, we show $\tilde{\sigma}_0^2$ and $\hat{\tilde{\sigma}}_0^2$ versus the number of snapshots N for the no-mismatch case; hence, $\Delta = 0$ in (58), and consequently, $\epsilon_0 = 0$. Note that the power estimates obtained by using $\hat{\mathbf{R}}$ approach those computed via $\mathbf{R}$ as N increases and that our RCB converges much faster than the SCB. The SCB requires that N is greater than or equal to the number of array sensors $M = 10$. However, our RCB works well even when N is as small as $N = 2$.

Fig. 2 shows the beampatterns of the SCB and RCB using $\mathbf{R}$ as well as $\hat{\mathbf{R}}$ with $N = 10$, 100, and 8000 for the same case as in

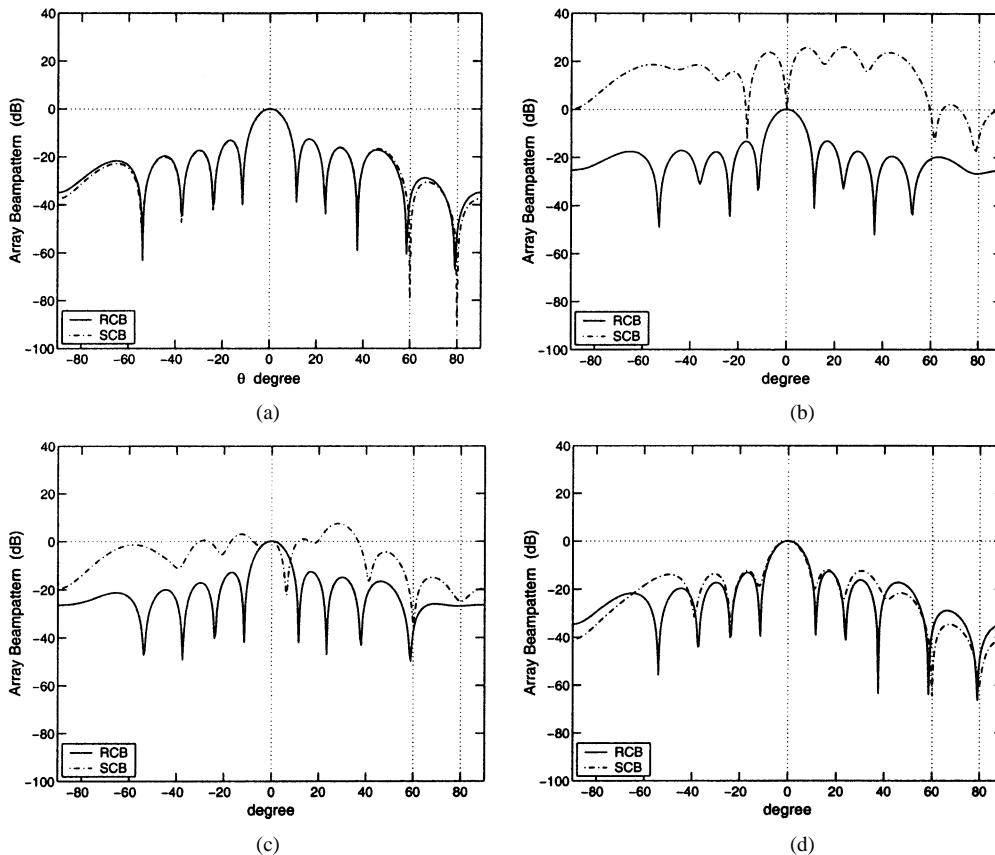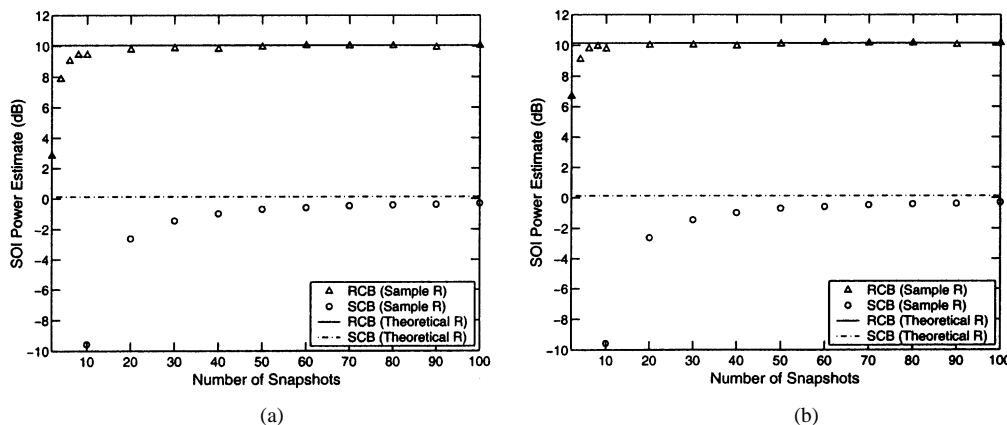Fig. 2.   Comparison of the beampatterns of SCB and RCB when $\epsilon = 3.5$ for (a) using $\mathbf{R}$, (b) using $\hat{\mathbf{R}}$ with $N = 10$, (c) using $\hat{\mathbf{R}}$ with $N = 100$, and (d) using $\hat{\mathbf{R}}$ with $N = 8000$. The true SOI power is 10 dB, and $\epsilon_0 = 0$ (i.e., no mismatch).

Fig. 3. $\bar{\sigma}_0^2$ (SCB using $\hat{\mathbf{R}}$ and $\mathbf{R}$) and $\hat{\bar{\sigma}}_0^2$ (RCB using $\hat{\mathbf{R}}$ and $\mathbf{R}$) versus N for (a) $\epsilon = 2.5$ and (b) $\epsilon = 4.5$. The true SOI power is 10 dB, and $\epsilon_0 = 3.2460$ (corresponding to $\Delta = 2.0°$).

Fig. 1. Note that the weight vectors used to calculate the beampatterns of RCB in this example (as well as in the following examples) are obtained by using the scaled estimate of the array steering vector $\sqrt{M}\hat{\mathbf{a}}_0/\|\hat{\mathbf{a}}_0\|$ in (32) instead of $\hat{\mathbf{a}}_0$. The vertical dotted lines in the figure denote the directions of arrival of the SOI as well as the interferences. The horizontal dotted lines in the figure correspond to 0 dB. Note from Fig. 2(a) that although the RCB beampatterns do not have nulls at the directions of arrival of the interferences as deep as those of the SCB, the interferences (whose powers are 20 dB) are sufficiently suppressed by the RCB to not disturb the SOI power estimation. Regarding the poor performance of SCB

for small N, note that the error between $\hat{\mathbf{R}}$ and $\mathbf{R}$ can be viewed as due to a steering vector error [24].

Figs. 3 and 4 are similar to Figs. 1 and 2, except that now the mismatch is $\Delta = 2°$ and accordingly $\epsilon_0 = 3.2460$. We note from Fig. 3 that even a relatively small Δ can cause a significant degradation of the SCB performance. As can be seen from Fig. 4, the SOI is considered to be an interference by SCB, and hence, it is suppressed. On the other hand, the SOI is preserved by our RCB and the performance of $\hat{\bar{\sigma}}_0^2$ obtained via our approach is quite good for a wide range of values of ϵ. Note that the RCB also has a smaller "noise gain" than the SCB.
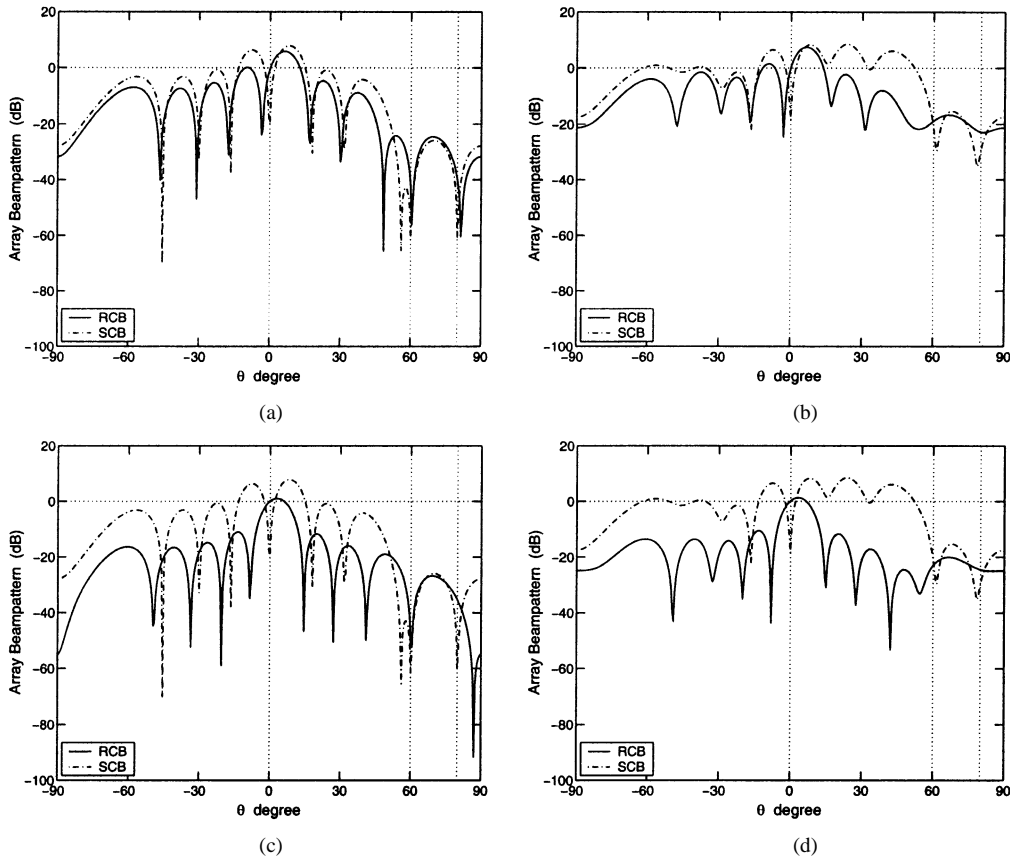
Fig. 4. Comparison of the beampatterns of SCB and RCB when $\epsilon = 1.0$ for (a) using $\mathbf{R}$ and (b) using $\hat{\mathbf{R}}$ with $N = 10$ and when $\epsilon = 4.5$ for (c) using $\mathbf{R}$ and (d) using $\hat{\mathbf{R}}$ with $N = 10$. The true SOI power is 10 dB, and $\epsilon_0 = 3.2460$ (corresponding to $\Delta = 2.0°$).

In Fig. 5, we compare the performance of our RCB with a fixed diagonal loading level-based approach. Specifically, the fixed loading level was chosen equal to ten times the noise power (assuming the knowledge of the noise power). Consider the same case as Fig. 4(d), except that now, we assume that $\mathbf{R}$ is available, and we vary the SNR by changing the SOI or noise power. For Fig. 5(a), (c), and (e), we fix the noise power at 0 dB and vary the SOI power between -10 and 20 dB. For Fig. 5(b), (d), and (f), we fix the SOI power at 10 dB and vary the noise power between -10 and 20 dB. Fig. 5(a) and (b) shows the diagonal loading levels of our RCB as functions of the SNR. Fig. 5(c) and (d) shows the SINRs of our RCB and the fixed diagonal loading level approach, and Fig. 5(e) and (f) shows the corresponding SOI power estimates, all as functions of the SNR. Note from Fig. 5(a) and (b) that our RCB adjusts the diagonal loading level adaptively as the SNR changes. It is obvious from Fig. 5 that our RCB significantly outperforms the fixed diagonal loading level approach when the SNR is medium or high.

We next consider an imaging example, where we wish to determine the incident signal power as a function of the steering direction θ. We assume that there are five incident signals with powers 30, 15, 40, 35, and 20 dB from directions $-35°$, $-15°$, $0°$, $10°$, and $40°$, respectively. To simulate the array calibration error, each element of the steering vector for each incident signal is perturbed with a zero-mean circularly symmetric complex Gaussian random variable so that the squared Euclidean norm of the difference between the true steering vector and the assumed one is 0.05. The perturbing

Gaussian random variables are independent of each other. Fig. 6 shows the power estimates of SCB and RCB that are obtained using $\mathbf{R}$ as a function of the direction angle for several values of ϵ. The small circles denote the true (direction of arrival, power)-coordinates of the five incident signals. Fig. 6 also shows the power estimates obtained with the data-independent beamformer using the assumed array steering vector divided by M as the weight vector. This approach is referred to as the delay-and-sum beamformer. We note that SCB can still give good direction-of-arrival estimates for the incident signals based on the peak power locations. However, the SCB estimates of the incident signal powers are way off. On the other hand, our RCB provides excellent power estimates of the incident sources and can also be used to determine their directions of arrival based on the peak locations. The delay-and-sum beamformer, however, has much poorer resolution than both SCB and RCB. Moreover, the sidelobes of the former give false peaks.

Finally, we examine the effects of the spherical and flat ellipsoidal constraints on SOI power estimation. We consider SOI power estimation in the presence of several strong interferences. We will vary the number of interferences from $K = 1$ to $K = 8$. The power of SOI is $\sigma_0^2 = 20$ dB, and the interference powers are $\sigma_1^2 = \cdots = \sigma_K^2 = 40$ dB. The SOI and interference directions of arrival are $\theta_0 = 10°$, $\theta_1 = -75°$, $\theta_2 = -60°$, $\theta_3 = -45°$, $\theta_4 = -30°$, $\theta_5 = -10°$, $\theta_6 = 25°$, $\theta_7 = 35°$, and $\theta_8 = 50°$. We assume that there is a look direction mismatch corresponding to $\Delta = 2°$, and accordingly, $\epsilon_0 = 3.1349$.
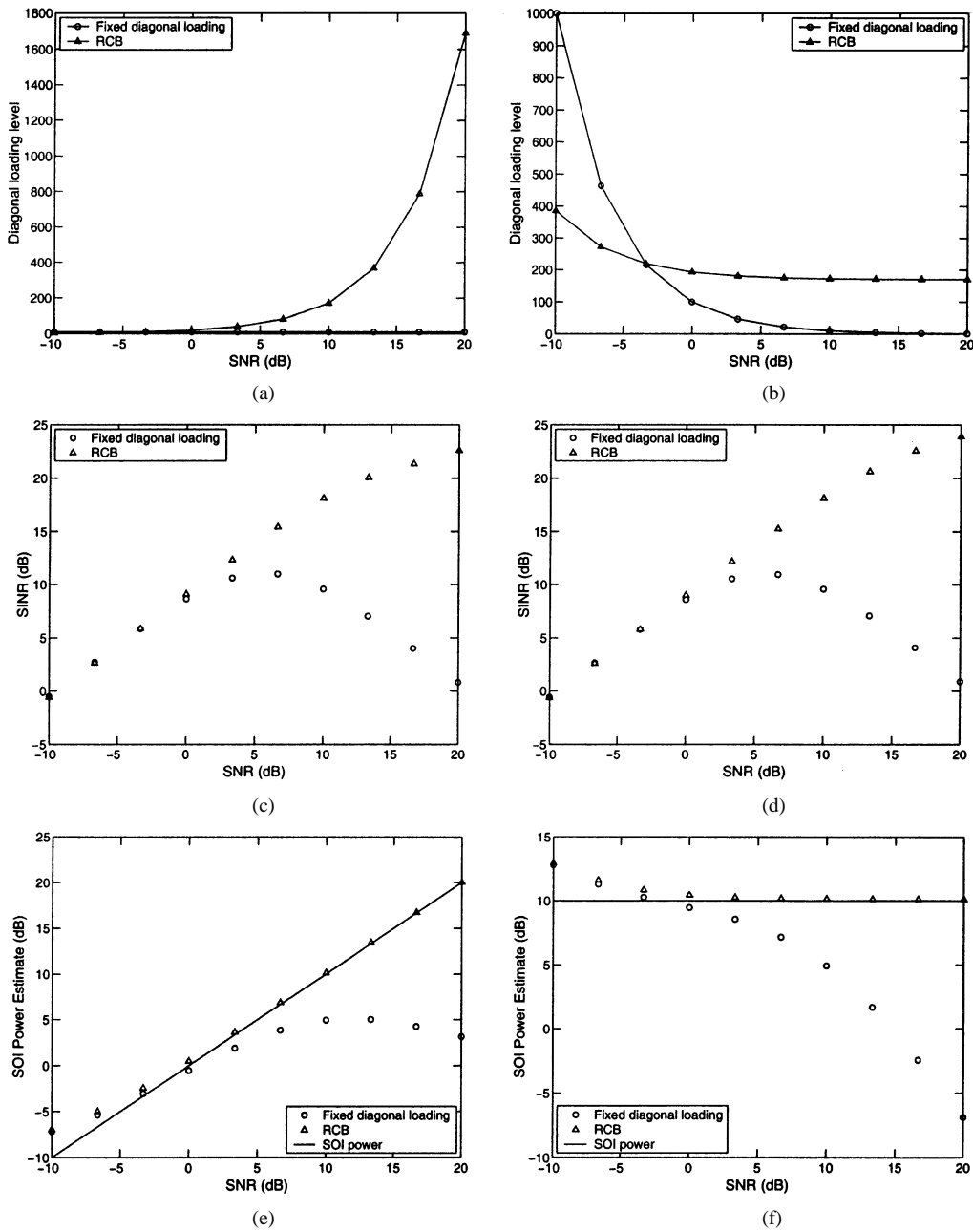
Fig. 5.   Comparison of a fixed diagonal loading level approach and our RCB when $\epsilon = 4.5$ and $\epsilon_0 = 3.2460$ (corresponding to $\Delta = 2.0°$).
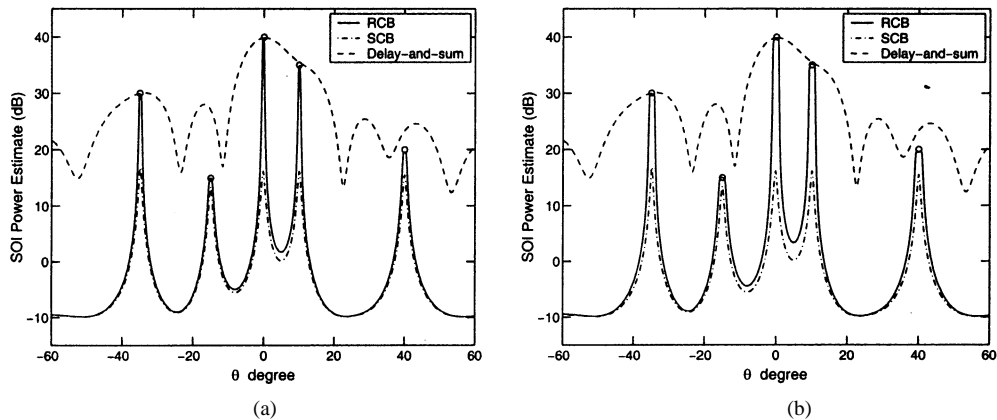

Fig. 6.   Power estimates (using $\mathbf{R}$) versus the steering direction θ when (a) $\epsilon = 0.03$ and (b) $\epsilon = 0.1$. The true powers of the incident signals from $-35°$, $-15°$, $0°$, $10°$, and $40°$ are denoted by circles, and $\epsilon_0 = 0.05$.
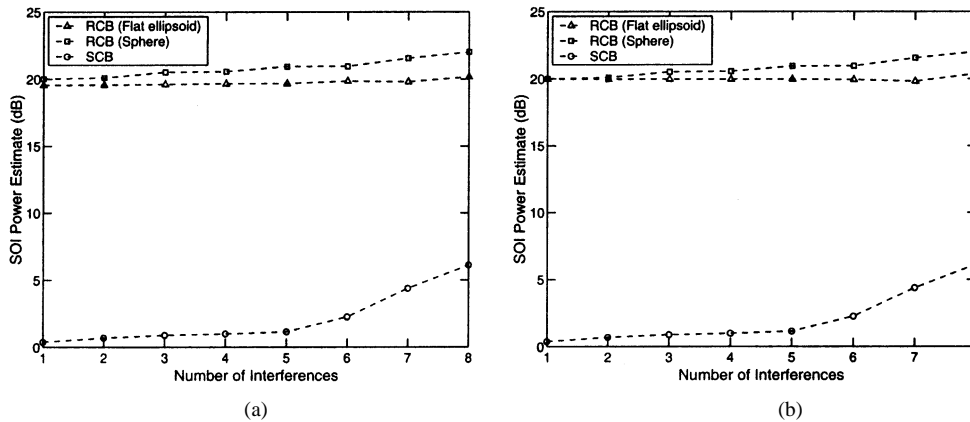
Fig. 7. $\bar{\sigma}_0^2$ (SCB), $\hat{\bar{\sigma}}_0^2$ (RCB with flat ellipsoidal constraint with $L = 2$), and $\hat{\sigma}_0^2$ (RCB with spherical constraint), based on $\mathbf{R}$, versus the number of interferences K when (a) $\delta = 1.8°$ and (b) $\delta = 2.4°$. The true SOI power is 20 dB, and $\epsilon_0 = 3.1349$ (corresponding to $\Delta = 2°$).

Fig. 7 shows the SOI power estimates, as a function of the number of interferences K, obtained by using SCB, RCB (with flat ellipsoidal constraint), and the more conservative RCB (with spherical constraint) all based on the theoretical array covariance matrix $\mathbf{R}$. For the RCB with flat ellipsoidal constraint, we let $\mathbf{B}$ contain two columns with the first column being $\mathbf{a}(\theta_0 + \Delta) - \mathbf{a}(\theta_0 + \Delta - \delta)$ and the second column being $\mathbf{a}(\theta_0 + \Delta) - \mathbf{a}(\theta_0 + \Delta + \delta)$. Note that choosing $\delta = \Delta = 2°$ gives the smallest flat ellipsoid that this $\mathbf{B}$ can offer to include $\mathbf{a}(\theta_0)$. However, we do not know the exact look-direction mismatch in practice. We choose $\delta = 1.8°$ and $\delta = 2.4°$ in Fig. 7(a) and (b), respectively. For RCB with spherical constraint, we choose ϵ to be the larger of $\|\mathbf{a}(\theta_0 + \Delta) - \mathbf{a}(\theta_0 + \Delta - \delta)\|^2$ and $\|\mathbf{a}(\theta_0 + \Delta) - \mathbf{a}(\theta_0 + \Delta + \delta)\|^2$. Note that RCB with flat ellipsoidal constraint and RCB with spherical constraint perform similarly when K is small. However, the former is more accurate than the latter for large K. Fig. 8 gives the beampatterns of the SCB and RCBs using $\mathbf{R}$, as well as $\hat{\mathbf{R}}$ with $N = 10$ for various K. For large K, the more conservative RCB with spherical constraint amplifies the SOI while attempting to suppress the interferences, as shown in Fig. 8. On the other hand, the RCB with flat ellipsoidal constraint maintains an approximate unity gain for the SOI and provides much deeper nulls for the interferences than the RCB with spherical constraint at a cost of worse noise gain. As compared with the RCBs, the SCB performs poorly as it attempts to suppress the SOI. Comparing Fig. 8(b) with 8(a), we note that for small K and N, RCB with spherical constraint has a much better noise gain than RCB with flat ellipsoidal constraint, which has a better noise gain than SCB. From Fig. 8(d), we note that for large K and small N, RCB with flat ellipsoidal constraint places deeper nulls at the interference angles than the more conservative RCB with spherical constraint. Fig. 9 shows the SOI power estimates versus the number of snapshots N for $K = 1$ and $K = 8$ when the sample covariance matrix $\hat{\mathbf{R}}$ is used in the beamformers. Note that for small K, RCB with spherical constraint converges faster than RCB with flat ellipsoidal constraint as N increases, whereas the latter converges faster than SCB. For large K, however, the convergence speeds of RCB with flat ellipsoidal constraint and RCB with spherical constraint are about the same as that of SCB; after convergence, the most accurate power estimate is provided by RCB with flat ellipsoidal constraint.

V. CONCLUSIONS

We have shown how to obtain a robust Capon beamformer (RCB) based on an ellipsoidal (including flat ellipsoidal) uncertainty set of the array steering vector at a comparable computational cost with that associated with SCB. The data-adaptive RCB is much less sensitive to steering vector mismatches than the standard Capon beamformer (SCB), and yet, it can retain the appealing properties of SCB including better resolution and much better interference rejection capability than the standard (data-independent) beamformer. We have shown that the RCB belongs to the class of diagonal loading approaches, but the amount of diagonal loading can be precisely calculated based on the uncertainty set of the steering vector. We have proven that despite the apparent differences between our RCB approach and the approaches presented in two recent publications, our RCB gives the same weight vector as the latter approaches, yet our RCB is computationally more efficient. The excellent performance of our RCB for SOI power estimation and imaging has been demonstrated via a number of numerical examples.

APPENDIX A
RELATIONSHIP BETWEEN OUR RCB AND THE RCB IN [8]

We repeat our optimization problem:

$$\min_{\mathbf{a}} \mathbf{a}^* \mathbf{R}^{-1} \mathbf{a}, \qquad \text{subject to } \|\mathbf{a} - \bar{\mathbf{a}}\|^2 = \epsilon. \qquad (59)$$

Let $\mathbf{a}_0$ denote the optimal solution of (59). Let

$$\mathbf{w}_0 = \frac{\mathbf{R}^{-1} \mathbf{a}_0}{\mathbf{a}_0^* \mathbf{R}^{-1} \mathbf{a}_0}. \qquad (60)$$

We show below that the $\mathbf{w}_0$ above is the optimal solution to the following SOCP considered in [8]:

$$\min_{\mathbf{w}} \mathbf{w}^* \mathbf{R} \mathbf{w}, \qquad \text{subject to } \mathbf{w}^* \bar{\mathbf{a}} \geq \sqrt{\epsilon} \|\mathbf{w}\| + 1$$
$$\text{Im}(\mathbf{w}^* \bar{\mathbf{a}}) = 0. \qquad (61)$$

First, we show that if $\|\bar{\mathbf{a}}\| \leq \sqrt{\epsilon}$, then there is no $\mathbf{w}$ that satisfies $\mathbf{w}^* \bar{\mathbf{a}} \geq \sqrt{\epsilon} \|\mathbf{w}\| + 1$. By using the Cauchy–Schwarz inequality, we have

$$\sqrt{\epsilon} \|\mathbf{w}\| + 1 \leq \mathbf{w}^* \bar{\mathbf{a}} \leq \sqrt{\epsilon} \|\mathbf{w}\| \qquad (62)$$
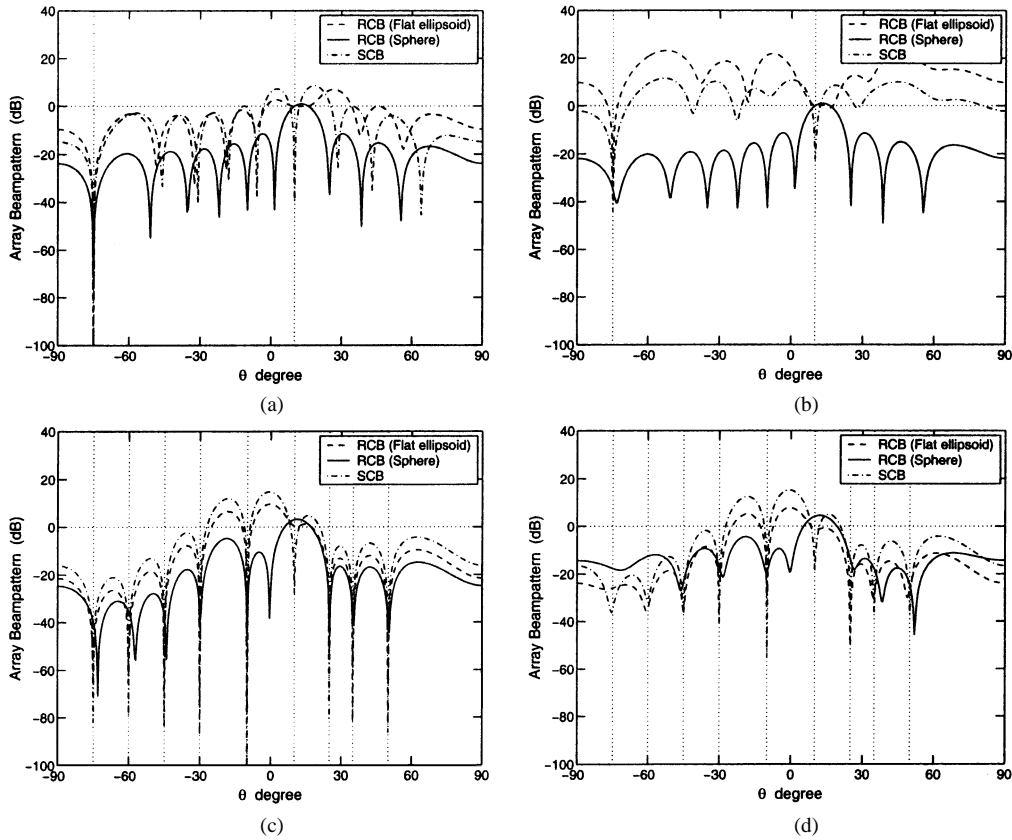
Fig. 8. Comparison of the beampatterns of SCB, RCB (with flat ellipsoidal constraint), and RCB (with spherical constraint) when $\delta = 2.4°$ for (a) $K = 1$ and using $\mathbf{R}$, (b) $K = 1$ and using $\hat{\mathbf{R}}$ with $N = 10$, (c) $K = 8$ and using $\mathbf{R}$, and (d) $K = 8$ and using $\hat{\mathbf{R}}$ with $N = 10$. The true SOI power is 20 dB, and $\epsilon_0 = 3.1349$ (corresponding to $\Delta = 2°$).
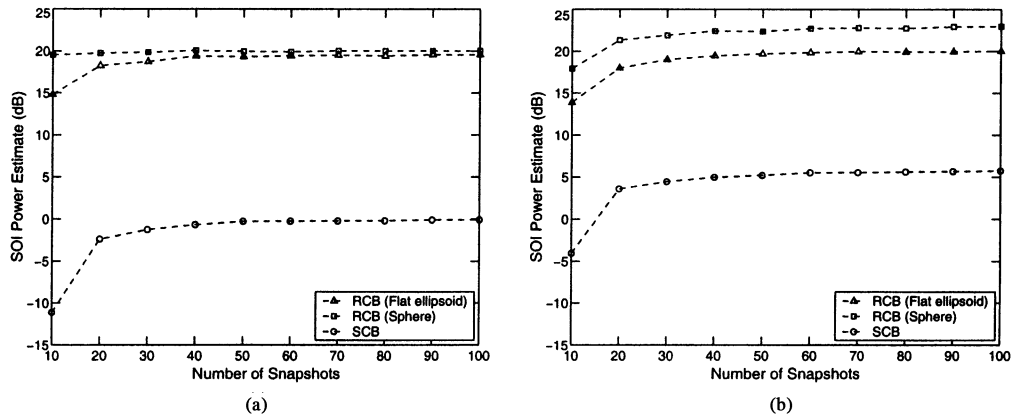

Fig. 9. Comparison of the SOI power estimates versus N obtained using SCB, RCB (with flat ellipsoidal constraint), and RCB (with spherical constraint), all with $\hat{\mathbf{R}}$, when $\delta = 2.4°$ for (a) $K = 1$ and (b) $K = 8$. The true SOI power is 20 dB, and $\epsilon_0 = 3.1349$ (corresponding to $\Delta = 2°$).

which is impossible. Hence, the constraint in (15), which is needed for our RCB to avoid the trivial solution, must also be satisfied by the RCB in [8].

Next, let

$$\mathbf{w} = \mathbf{w}_0 + \mathbf{y}. \qquad (63)$$

We show below that the solution of (61) corresponds to $\mathbf{y} = \mathbf{0}$.

Insertion of (63) in (61) gives

$$\min_{\mathbf{y}} \mathbf{y}^*\mathbf{R}\mathbf{y} + \frac{2}{\mathbf{a}_0^*\mathbf{R}^{-1}\mathbf{a}_0} \mathrm{Re}(\mathbf{y}^*\mathbf{a}_0) + \frac{1}{\mathbf{a}_0^*\mathbf{R}^{-1}\mathbf{a}_0} \qquad (64)$$

subject to

$$\mathbf{y}^*\overline{\mathbf{a}} + \mathbf{w}_0^*\overline{\mathbf{a}} - \sqrt{\epsilon}\|\mathbf{w}_0 + \mathbf{y}\| \geq 1 \qquad (65)$$

and

$$\mathrm{Im}(\mathbf{w}_0^*\overline{\mathbf{a}} + \mathbf{y}^*\overline{\mathbf{a}}) = 0. \qquad (66)$$

Let

$$\overline{\mathbf{a}} = \mathbf{a}_0 + \boldsymbol{\mu}. \qquad (67)$$

Then, (65) and (66), respectively, become

$$\mathbf{y}^*\mathbf{a}_0 + \mathbf{y}^*\boldsymbol{\mu} + \mathbf{w}_0^*\boldsymbol{\mu} \geq \sqrt{\epsilon}\|\mathbf{w}_0 + \mathbf{y}\| \tag{68}$$

and

$$\mathrm{Im}(\mathbf{w}_0^*\boldsymbol{\mu} + \mathbf{y}^*\mathbf{a}_0 + \mathbf{y}^*\boldsymbol{\mu}) = 0 \tag{69}$$

which implies that

$$\mathrm{Re}(\mathbf{y}^*\mathbf{a}_0) \geq \sqrt{\epsilon}\|\mathbf{w}_0 + \mathbf{y}\| - \mathrm{Re}(\mathbf{y}^*\boldsymbol{\mu} + \mathbf{w}_0^*\boldsymbol{\mu}). \tag{70}$$

Since

$$\begin{aligned}
|\mathrm{Re}[(\mathbf{y} + \mathbf{w}_0)^*\boldsymbol{\mu}]| &\leq |(\mathbf{y} + \mathbf{w}_0)^*\boldsymbol{\mu}| \\
&\leq \|\mathbf{y} + \mathbf{w}_0\|\,\|\boldsymbol{\mu}\| \\
&= \sqrt{\epsilon}\|\mathbf{w}_0 + \mathbf{y}\|
\end{aligned} \tag{71}$$

it follows from (70) that

$$\mathrm{Re}(\mathbf{y}^*\mathbf{a}_0) \geq 0. \tag{72}$$

This implies at once that the minimizer of (64) is $\mathbf{y} = \mathbf{0}$, provided that we can show that $\mathbf{y} = \mathbf{0}$ satisfies the constraints (65) and (66) or, equivalently, (68) and (69), that is

$$\mathrm{Re}(\mathbf{w}_0^*\boldsymbol{\mu}) \geq \sqrt{\epsilon}\|\mathbf{w}_0\| \tag{73}$$

and

$$\mathrm{Im}(\mathbf{w}_0^*\boldsymbol{\mu}) = 0. \tag{74}$$

Inserting (60) in (73) yields

$$\mathrm{Re}\left(\mathbf{a}_0^*\mathbf{R}^{-1}\boldsymbol{\mu}\right) \geq \sqrt{\epsilon\mathbf{a}_0^*\mathbf{R}^{-2}\mathbf{a}_0}. \tag{75}$$

Using (60) in (74) gives

$$\mathrm{Im}\left(\mathbf{a}_0^*\mathbf{R}^{-1}\boldsymbol{\mu}\right) = 0. \tag{76}$$

To prove (75) and (76), we need to analyze (59). By using the Lagrange multiplier theory, we obtain [see (18)]

$$\mathbf{R}^{-1}\mathbf{a}_0 + \lambda(\mathbf{a}_0 - \bar{\mathbf{a}}) = \mathbf{0} \tag{77}$$

where $\lambda \geq 0$ is the Lagrange multiplier. Using (67) in (77) yields

$$\mathbf{R}^{-1}\mathbf{a}_0 = \lambda\boldsymbol{\mu}. \tag{78}$$

Using (78) in (75) gives

$$\mathrm{Re}\left(\lambda\|\boldsymbol{\mu}\|^2\right) = \lambda\|\boldsymbol{\mu}\|^2 \geq \sqrt{\epsilon}\lambda\|\boldsymbol{\mu}\|. \tag{79}$$

However, due to the constraint in (59), i.e., $\|\boldsymbol{\mu}\|^2 = \epsilon$, (79) is satisfied with equality, which proves that (75) is satisfied with equality. This means that the first constraint in (61) is satisfied with equality and, hence, that the optimal solution to (61) also occurs at the boundary of its constraint set, as expected (see also [9]). Using (78) in (76) proves (76) since

$$\mathrm{Im}\left(\lambda\|\boldsymbol{\mu}\|^2\right) = 0. \tag{80}$$

APPENDIX B
CALCULATING THE STEERING VECTOR FROM THE OPTIMAL WEIGHT VECTOR

We now show how to obtain the steering vector $\mathbf{a}_0$ from the optimal solution $\mathbf{w}_0$ of the SOCP (61). In Appendix A, we have shown that

$$\mathbf{w}_0 = \frac{\mathbf{R}^{-1}\mathbf{a}_0}{\mathbf{a}_0^*\mathbf{R}^{-1}\mathbf{a}_0}. \tag{81}$$

Hence

$$\mathbf{w}_0^*\mathbf{R}\mathbf{w}_0 = \frac{1}{\mathbf{a}_0^*\mathbf{R}^{-1}\mathbf{a}_0} \tag{82}$$

which, along with (81), leads to

$$\mathbf{a}_0 = \frac{\mathbf{R}\mathbf{w}_0}{\mathbf{w}_0^*\mathbf{R}\mathbf{w}_0}. \tag{83}$$

Hence, from the optimal solution $\mathbf{w}_0$ of the SOCP (61), we can obtain the $\mathbf{a}_0$ as above and then correct the scaling ambiguity problem of the SOI power estimation in the same way as in our RCB approach [see (28)].

APPENDIX C
RELATIONSHIP BETWEEN OUR RCB AND THE RCB IN [9]

Consider the SOCP with the ellipsoidal (including flat ellipsoidal) constraint on $\mathbf{w}$ and not on $\mathbf{a}$ as in our formulation, which is considered in [9]:

$$\min_{\mathbf{w}} \mathbf{w}^*\mathbf{R}\mathbf{w} \quad \text{subject to } \|\mathbf{B}^*\mathbf{w}\| \leq \bar{\mathbf{a}}^*\mathbf{w} - 1. \tag{84}$$

The Lagrange multiplier approach gives the optimal solution [9]

$$\begin{aligned}
\hat{\mathbf{w}} &= -\left[\frac{\mathbf{R}}{\gamma} + (\mathbf{B}\mathbf{B}^* - \bar{\mathbf{a}}\bar{\mathbf{a}}^*)\right]^{-1}\bar{\mathbf{a}} \\
&= -\left(\frac{\mathbf{R}}{\gamma} + \mathbf{B}\mathbf{B}^*\right)^{-1}\bar{\mathbf{a}} \\
&\quad - \frac{\left(\frac{\mathbf{R}}{\gamma} + \mathbf{B}\mathbf{B}^*\right)^{-1}\bar{\mathbf{a}}\bar{\mathbf{a}}^*\left(\frac{\mathbf{R}}{\gamma} + \mathbf{B}\mathbf{B}^*\right)^{-1}\bar{\mathbf{a}}}{1 - \bar{\mathbf{a}}^*\left(\frac{\mathbf{R}}{\gamma} + \mathbf{B}\mathbf{B}^*\right)^{-1}\bar{\mathbf{a}}} \\
&= \frac{\left(\frac{\mathbf{R}}{\gamma} + \mathbf{B}\mathbf{B}^*\right)^{-1}\bar{\mathbf{a}}}{\bar{\mathbf{a}}^*\left(\frac{\mathbf{R}}{\gamma} + \mathbf{B}\mathbf{B}^*\right)^{-1}\bar{\mathbf{a}} - 1} \\
&= \frac{(\mathbf{R} + \gamma\mathbf{B}\mathbf{B}^*)^{-1}\bar{\mathbf{a}}}{\bar{\mathbf{a}}^*(\mathbf{R} + \gamma\mathbf{B}\mathbf{B}^*)^{-1}\bar{\mathbf{a}} - \frac{1}{\gamma}}
\end{aligned} \tag{85}$$

where γ is the unique solution of

$$\begin{aligned}
h(\gamma) &= \gamma^2\bar{\mathbf{a}}^*(\mathbf{R} + \gamma\mathbf{P})^{-1}\mathbf{P}(\mathbf{R} + \gamma\mathbf{P})^{-1}\bar{\mathbf{a}} \\
&\quad - 2\gamma\bar{\mathbf{a}}^*(\mathbf{R} + \gamma\mathbf{P})^{-1}\bar{\mathbf{a}} - 1 = 0
\end{aligned} \tag{86}$$

and $\mathbf{P} = \mathbf{B}\mathbf{B}^* - \bar{\mathbf{a}}\bar{\mathbf{a}}^*$ [to obtain (85), we have used the matrix inversion lemma]. Note that solving for the Lagrange multiplier from (86), as discussed in [9], is more complicated than solving our counterpart in (52).

To prove that the weight vectors in (56) and (85) are the same, we first prove that for the $\check{\lambda}$ satisfying (49), we have

$$h\left(\frac{1}{\check{\lambda}}\right) = 0. \tag{87}$$

To prove (87), note that

$$
\begin{aligned}
h\left(\frac{1}{\check{\lambda}}\right) &= \overline{\mathbf{a}}^*(\check{\lambda}\mathbf{R} + \mathbf{P})^{-1}(\mathbf{BB}^* - \overline{\mathbf{a}}\overline{\mathbf{a}}^*)(\check{\lambda}\mathbf{R} + \mathbf{P})^{-1}\overline{\mathbf{a}} \\
&\quad - 2\overline{\mathbf{a}}^*(\check{\lambda}\mathbf{R} + \mathbf{P})^{-1}\overline{\mathbf{a}} - 1 \\
&= \overline{\mathbf{a}}^*(\check{\lambda}\mathbf{R} + \mathbf{BB}^* - \overline{\mathbf{a}}\overline{\mathbf{a}}^*)^{-1} \\
&\quad \cdot \mathbf{BB}^*(\check{\lambda}\mathbf{R} + \mathbf{BB}^* - \overline{\mathbf{a}}\overline{\mathbf{a}}^*)^{-1}\overline{\mathbf{a}} \\
&\quad - \left[\overline{\mathbf{a}}^*(\check{\lambda}\mathbf{R} + \mathbf{BB}^* - \overline{\mathbf{a}}\overline{\mathbf{a}}^*)^{-1}\overline{\mathbf{a}} + 1\right]^2. \tag{88}
\end{aligned}
$$

Since [see (85)]

$$
(\check{\lambda}\mathbf{R} + \mathbf{BB}^* - \overline{\mathbf{a}}\overline{\mathbf{a}}^*)^{-1}\overline{\mathbf{a}} = \frac{(\check{\lambda}\mathbf{R} + \mathbf{BB}^*)^{-1}\overline{\mathbf{a}}}{1 - \overline{\mathbf{a}}^*(\check{\lambda}\mathbf{R} + \mathbf{BB}^*)^{-1}\overline{\mathbf{a}}} \tag{89}
$$

we can write $h(1/\check{\lambda})$ as a fraction whose numerator is

$$
\begin{aligned}
\tilde{h}\left(\frac{1}{\check{\lambda}}\right) &= \overline{\mathbf{a}}^*(\check{\lambda}\mathbf{R} + \mathbf{BB}^*)^{-1}\mathbf{BB}^*(\check{\lambda}\mathbf{R} + \mathbf{BB}^*)^{-1}\overline{\mathbf{a}} - 1 \\
&= \left\|\mathbf{B}^*(\check{\lambda}\mathbf{R} + \mathbf{BB}^*)^{-1}\overline{\mathbf{a}}\right\|^2 - 1. \tag{90}
\end{aligned}
$$

Since $\check{\lambda}$ satisfies (49), we have that

$$
\begin{aligned}
1 &= \left\|(\check{\mathbf{R}} + \check{\lambda}\mathbf{I})^{-1}\overline{\overline{\mathbf{a}}}\right\|^2 \\
&= \left\|(\mathbf{B}^*\mathbf{R}^{-1}\mathbf{B} + \check{\lambda}\mathbf{I})^{-1}\mathbf{B}^*\mathbf{R}^{-1}\overline{\mathbf{a}}\right\|^2 \\
&= \left\|\frac{1}{\check{\lambda}}\left[\mathbf{I} - \mathbf{B}^*(\check{\lambda}\mathbf{R} + \mathbf{BB}^*)^{-1}\mathbf{B}\right]\mathbf{B}^*\mathbf{R}^{-1}\overline{\mathbf{a}}\right\|^2 \\
&= \left\|\mathbf{B}^*\left[\mathbf{I} - (\check{\lambda}\mathbf{R} + \mathbf{BB}^*)^{-1}\mathbf{BB}^*\right](\check{\lambda}\mathbf{R})^{-1}\overline{\mathbf{a}}\right\|^2 \\
&= \left\|\mathbf{B}^*(\check{\lambda}\mathbf{R} + \mathbf{BB}^*)^{-1}\left[\check{\lambda}\mathbf{R} + \mathbf{BB}^* - \mathbf{BB}^*\right](\check{\lambda}\mathbf{R})^{-1}\overline{\mathbf{a}}\right\|^2 \\
&= \left\|\mathbf{B}^*(\check{\lambda}\mathbf{R} + \mathbf{BB}^*)^{-1}\overline{\mathbf{a}}\right\|^2 \tag{91}
\end{aligned}
$$

which proves (87).

Next, we prove that the denominators of (56) and (85) are the same. The denominator of (56) can be written as

$$
\begin{aligned}
&\overline{\mathbf{a}}^*\left(\mathbf{R} + \frac{1}{\check{\lambda}}\mathbf{BB}^*\right)^{-1}\left(\mathbf{R} + \frac{1}{\check{\lambda}}\mathbf{BB}^* - \frac{1}{\check{\lambda}}\mathbf{BB}^*\right) \\
&\quad \cdot \left(\mathbf{R} + \frac{1}{\check{\lambda}}\mathbf{BB}^*\right)^{-1}\overline{\mathbf{a}} \\
&= \overline{\mathbf{a}}^*\left(\mathbf{R} + \frac{1}{\check{\lambda}}\mathbf{BB}^*\right)^{-1}\overline{\mathbf{a}} - \check{\lambda}\left\|\mathbf{B}^*(\check{\lambda}\mathbf{R} + \mathbf{BB}^*)^{-1}\overline{\mathbf{a}}\right\|^2 \\
&= \overline{\mathbf{a}}^*\left(\mathbf{R} + \frac{1}{\check{\lambda}}\mathbf{BB}^*\right)^{-1}\overline{\mathbf{a}} - \check{\lambda} \tag{92}
\end{aligned}
$$

where we have used (91). Since for the $\check{\lambda}$ satisfying (49) and γ satisfying (86), $\check{\lambda} = 1/\gamma$, and the proof is concluded.

REFERENCES

[1] P. Stoica and R. L. Moses, *Introduction to Spectral Analysis*. Englewood Cliffs, NJ: Prentice-Hall, 1997.

[2] H. L. Van Trees, *Detection, Estimation, and Modulation Theory, Part IV, Optimum Array Processing*. New York: Wiley, 2002.

[3] J. Capon, "High resolution frequency-wavenumber spectrum analysis," *Proc. IEEE*, vol. 57, pp. 1408–1418, Aug. 1969.

[4] R. T. Lacoss, "Data adaptive spectral analysis methods," *Geophys.*, vol. 36, no. 4, pp. 661–675, Aug. 1971.

[5] C. D. Seligson, "Comments on high resolution frequency-wavenumber spectrum analysis," *Proc. IEEE*, vol. 58, pp. 947–949, 1970.

[6] H. Cox, "Resolving power and sensitivity to mismatch of optimum array processors," *J. Acoust. Soc. Amer.*, vol. 54, no. 3, pp. 771–785, 1973.

[7] A. B. Gershman, "Robust adaptive beamforming in sensor arrays," *Int. J. Electron. Commun.*, vol. 53, no. 6, pp. 305–314, 1999.

[8] S. A. Vorobyov, A. B. Gershman, and Z.-Q. Luo, "Robust adaptive beamforming using worst-case performance optimization," IEEE Trans. Signal Processing, vol. 51, pp. 313–324, Feb. 2003, to be published.

[9] R. G. Lorenz and S. P. Boyd, "Robust minimum variance beamforming," IEEE Trans. Signal Processing, 2001, submitted for publication.

[10] O. L. Frost III, "An algorithm for linearly constrained adaptive array processing," *Proc. IEEE*, vol. 60, pp. 926–935, Aug. 1972.

[11] M. H. Er and A. Cantoni, "Derivative constraints for broad-band element space antenna array processors," *IEEE Trans. Acoust., Speech, Signal Processing*, vol. ASSP–31, pp. 1378–1393, Dec. 1983.

[12] K. M. Buckley and L. J. Griffiths, "An adaptive generalized sidelobe canceller with derivative constraints," *IEEE Trans. Antennas Propagat.*, vol. AP–34, pp. 311–319, Mar. 1986.

[13] S. Zhang and I. L. Thng, "Robust presteering derivative constraints for broadband antenna arrays," *IEEE Trans. Signal Processing*, vol. 50, pp. 1–10, Jan. 2002.

[14] M. Zatman, "Comments on theory and applications of covariance matrix tapers for robust adaptive beamforming," *IEEE Trans. Signal Processing*, vol. 48, pp. 1796–1800, June 2000.

[15] J. E. Hudson, *Adaptive Array Principles*. London, U.K.: Peter Peregrinus, 1981.

[16] Y. I. Abramovich and A. I. Nevrev, "An analysis of effectiveness of adaptive maximization of the signal-to-noise ratio which utilizes the inversion of the estimated correlation matrix," *Radio Eng. Electron. Phys.*, vol. 26, pp. 67–74, Dec. 1981.

[17] M. H. Er and A. Cantoni, "An alternative formulation for an optimum beamformer with robustness capability," in *Proc. Inst. Elect. Eng. F, Commun., Radar, Signal Process.*, vol. 132, 1985, pp. 447–460.

[18] H. Cox, R. M. Zeskind, and M. M. Owen, "Robust adaptive beamforming," *IEEE Trans. Acoust., Speech, Signal Processing*, vol. ASSP-35, pp. 1365–1376, Oct. 1987.

[19] B. D. Carlson, "Covariance matrix estimation errors and diagonal loading in adaptive arrays," *IEEE Trans. Aerosp. Electron. Syst.*, vol. 24, pp. 397–401, July 1988.

[20] B. D. Van Veen, "Minimum variance beamforming with soft response constraints," *IEEE Trans. Signal Processing*, vol. 39, pp. 1964–1972, Sept. 1991.

[21] R. Wu, Z. Bao, and Y. Ma, "Control of peak sidelobe level in adaptive arrays," *IEEE Trans. Antennas Propagat.*, vol. 44, pp. 1341–1347, Oct. 1996.

[22] C.-C. Lee and J.-H. Lee, "Robust adaptive array beamforming under steering vector errors," *IEEE Trans. Antennas Propagat.*, vol. 45, pp. 168–175, Jan. 1997.

[23] Z. Tian, K. L. Bell, and H. L. Van Trees, "A recursive least squares implementation for LCMP beamforming under quadratic constraints," *IEEE Trans. Signal Processing*, vol. 49, pp. 1138–1145, June 2001.

[24] D. D. Feldman and L. J. Griffiths, "A projection approach for robust adaptive beamforming," *IEEE Trans. Signal Processing*, vol. 42, pp. 867–876, Apr. 1994.

[25] S. Q. Wu and J. Y. Zhang, "A new robust beamforming method with antennae calibration errors," in *Proc. IEEE Wireless Commun. Networking Conf.*, vol. 2, New Orleans, LA, Sept. 1999, pp. 869–872.

[26] P. Stoica, Z. Wang, and J. Li, "Robust Capon beamforming," *IEEE Signal Processing Lett.*, June 2003, to be published.

[27] T. L. Marzetta, "A new interpretation for Capon's maximum likelihood method of frequency-wavenumber spectrum estimation," *IEEE Trans. Acoust., Speech, Signal Processing*, vol. 31, pp. 445–449, Apr. 1983.

[28] R. G. Lorenz and S. P. Boyd, "Robust beamforming in GPS Arrays," in *Proc. Inst. Navigat., Nat. Tech. Meet.*, Jan. 2002.

[29] J. F. Sturm, "Using SeDuMi 1.02, a MATLAB toolbox for optimization over symmetric cones," *Optim. Methods Software*, no. 11–12, pp. 625–653, 1999.

[30] A. V. Fiacco and G. P. McCormick, *Nonlinear Programming: Sequential Unconstrained Minimization Techniques*. New York: Wiley, 1968.

[31] M. Lobo, L. Vandenberghe, S. Boyd, and H. Lebret, "Applications of second-order cone programming," *Linear Algebra Applications, Special Issue on Linear Algebra in Control, Signals and Image Processing*, pp. 193–228, Nov. 1998.

[32] K.-B. Yu, "Recursive updating the eigenvalue decomposition of a covariance matrix," *IEEE Trans. Signal Processing*, vol. 39, pp. 1136–1145, May 1991.

[33] Y. Hua, M. Nikpour, and P. Stoica, "Optimal reduced-rank estimation and filtering," *IEEE Trans. Signal Processing*, vol. 49, pp. 457–469, Mar. 2001.

[34] D. C. Sorensen, "Newton's method with a model trust region modification," *SIAM J. Numerical Anal.*, vol. 19, no. 2, pp. 409–426, Apr. 1982.

Jian Li (S'87–M'91–SM'97) received the M.Sc. and Ph.D. degrees in electrical engineering from The Ohio State University (OSU), Columbus, in 1987 and 1991, respectively.

From April 1991 to June 1991, she was an Adjunct Assistant Professor with the Department of Electrical Engineering, OSU. From July 1991 to June 1993, she was an Assistant Professor with the Department of Electrical Engineering, University of Kentucky, Lexington. Since August 1993, she has been with the Department of Electrical and Computer Engineering, University of Florida, Gainesville, where she is currently a Professor. Her current research interests include spectral estimation, array signal processing, and their applications.

Dr. Li is a member of Sigma Xi and Phi Kappa Phi. She received the 1994 National Science Foundation Young Investigator Award and the 1996 Office of Naval Research Young Investigator Award. She was an Executive Committee Member of the 2002 International Conference on Acoustics, Speech, and Signal Processing, Orlando, FL, May 2002. She is presently a member of the Signal Processing Theory and Methods (SPTM) Technical Committee of the IEEE Signal Processing Society.

Petre Stoica (F'94) received the D.Sc. degree in automatic control from the Polytechnic Institute of Bucharest (BPI), Bucharest, Romania, in 1979 and an honorary doctorate degree in science from Uppsala University (UU), Uppsala, Sweden, in 1993.

He is Professor of system modeling with the Department of Systems and Control at UU. Previously, he was a Professor of system identification and signal processing with the Faculty of Automatic Control and Computers at BPI. He held longer visiting positions with Eindhoven University of Technology, Eindhoven, The Netherlands; Chalmers University of Technology, Gothenburg, Sweden (where he held a Jubilee Visiting Professorship); UU; The University of Florida, Gainesville; and Stanford University, Stanford, CA. His main scientific interests are in the areas of system identification, time series analysis and prediction, statistical signal and array processing, spectral analysis, wireless communications, and radar signal processing. He has published seven books, ten book chapters, and some 450 papers in archival journals and conference records on these topics. The most recent book he co-authored, with R. Moses, is entitled *Introduction to Spectral Analysis* (Englewood Cliffs, NJ: Prentice-Hall, 1997). Recently, he edited two books on signal processing advances in wireless communications and mobile communications (Englewood Cliffs, NJ: Prentice-Hall, 2001). He is on the editorial boards of five journals in the field: *Journal of Forecasting; Signal Processing*; *Circuits, Signals, and Signal Processing*; *Digital Signal Processing—A Review Journal*; and *Multidimensional Systems and Signal Processing*. He was a Co-Guest Editor for several special issues on system identification, signal processing, spectral analysis, and radar for some of the aforementioned journals, as well as for PROCEEDINGS OF THE IEEE.

Dr. Stoica was co-recipient of the IEEE ASSP Senior Award for a paper on statistical aspects of array signal processing. He was also recipient of the Technical Achievement Award of the IEEE Signal Processing Society for fundamental contributions to statistical signal processing with applications in time-series analysis, system identification, and array signal processing. In 1998, he was the recipient of a Senior Individual Grant Award of the Swedish Foundation for Strategic Research. He was also co-recipient of the 1998 EURASIP Best Paper Award for Signal Processing for a work on parameter estimation of exponential signals with time-varying amplitude, a 1999 IEEE Signal Processing Society Best Paper Award for a paper on parameter and rank estimation of reduced-rank regression, a 2000 IEEE Third Millennium Medal, and the 2000 W. R. G. Baker Prize Paper Award for a paper on maximum likelihood methods for radar. He was a member of the international program committees of many topical conferences. From 1981 to 1986, he was the Director of the International Time-Series Analysis and Forecasting Society, and he has been a member of the IFAC Technical Committee on Modeling, Identification, and Signal Processing since 1994. He is also a member of the Romanian Academy and a Fellow of the Royal Statistical Society.

Zhisong Wang (S'02) received the B.E. degree in electrical engineering from Tongji University, Shanghai, China, in 1998. Since May 2002, he has been a research assistant with the Department of Electrical and Computer Engineering, University of Florida, Gainesville, where he is pursuing Ph.D. degree in electrical engineering.

His current research interests include spectral estimation, array signal processing, and signal processing for acoustic and radar applications.